Study of a plug nozzle for supersonic aircraft concepts

Khairul B.M.Q. Zaman[1], John H. Korth[2], Amy F. Fagan[3] and James, E. Bridges[4]
NASA Glenn Research Center
Cleveland, OH 44135

A plug nozzle with a cylindrical cowl is studied. The geometry is adopted following commercial supersonic aircraft concepts considered in an ongoing NASA program. For the given cowl, plugs of different shapes are studied including straight conic shapes, shapes developed by a numerical optimization study for best thrust performance, as well as porous plugs. Experimental data on noise and flow field are discussed with an eye for minimum noise at low nozzle pressure ratios (NPR≈2) representing landing and takeoff (LTO) conditions. NPR up to about 4.7 is covered in the experiments. For the NPR range covered, results show that a plug designed for optimum thrust at cruise is noisier than a plug designed for optimum thrust at LTO. Limited thrust data with accompanying numerical simulation results are presented. Overall trends in thrust results from the numerical simulation show good agreement with the experimental data. The experiments also show that the plugs can generate transonic tones and excess broadband noise (EBBN) at low NPR, apart from well-known screech tones and broadband shock associated noise (BBSN) at high NPR. Interestingly, a long porous plug is found to effectively suppress all these aberrant noise components while suffering less than 1% loss in thrust coefficient.

1. Introduction

Nozzles with external plugs are candidates for the exhaust system of commercial supersonic aircraft concepts in an ongoing research program at NASA. As part of that effort, a fundamental study on plug nozzle design is being conducted at NASA Glenn Research Center (GRC). Experimental and limited numerical simulation results from this study, for a plug nozzle with a convergent aft cowl geometry, had been reported in recent publications [1, 2]. A detailed literature review on plug nozzles had been given in [1]. Conventional method-of-characteristics (MoC) design for the plug requires that the flow is choked at the nozzle exit. This is why a sharp convergence of the cowl is invoked for the design in most previous studies found in the literature [3-5], leading to the choice of the convergent cowl in our earlier study [2]. Such a cowl, however, is not suitable for supersonic flights because of large boattail drag suffered by its outer surface. The boattail drag consideration dictates that the cowl be more or less cylindrical in shape, and although various other shapes have been studied in the past by others (e.g., [6]), a cylindrical shape is currently adopted in the research program at NASA (earlier studies from this program are reported, e.g., in [7] and [8]). In addition to minimizing boattail drag, the cylindrical cowl shape may have other advantages. With the plug crown located inside, the flow experiences convergence and divergence as with a convergent-divergent (C-D) nozzle. By translating the plug, different throat-to-exit area ratio may be achieved to obtain full expansion at different nozzle pressure ratios (NPR). This offers a relatively easy active control strategy covering the entire flight regime from LTO to cruise conditions.

---

[1] Inlets & Nozzles Branch, AIAA Associate Fellow.
[2] Inlets & Nozzles Branch, AIAA Member.
[3] Optics & Photonics Branch, AIAA Associate Fellow.
[4] Acoustics Branch, AIAA Associate Fellow.

A smaller-scale model of the plug nozzle with cylindrical cowl, following the design in the NASA program, has been fabricated for continued fundamental study. All the plugs used with the earlier convergent cowl are readily adopted to this model. In addition, a few other plugs have been obtained following a numerical optimization study [9]. The various plugs are experimentally investigated for noise, flow fields as well as thrust with complementary numerical simulations. The noise data exhibit certain unique characteristics and the details of those are discussed with accompanying schlieren flow visualization. At present the uncertainty of the thrust data is large and only limited data are presented in this paper. Improvements in the thrust stand may allow for more accurate thrust data to be included in a future version of this paper for Journal publication.

2. Experimental Facility and Procedure

2.1 Jet facility and plug geometries

The experiments are conducted in an open jet facility at GRC [1, 2]. The experimental setup is shown in Fig. 1(a). The same setup is used to collect noise data, schlieren images as well as thrust data. For thrust measurement, the flow from a 'fixed plenum', annotated on the side of Fig. 1(a), is routed through four U-shaped tubes (inner diameter = 1.31"; all dimensions in this paper are given in inches). The flow enters radially into a 'floating plenum' that is mounted on a linear bearing allowing it to move freely in the axial direction. Each of the four feed tubes has a flexible component. The axial force experienced by the floating plenum due to the jet exhaust is measured by a load cell attached to the face of the fixed plenum. The displacement required by the load cell is very small, within a few thousandths of an inch. Thus, the nozzle exit location remains practically unchanged allowing the noise and schlieren measurements with the same test setup.

Since the flow enters the floating plenum radially, it has no axial force at the inlet and therefore the load cell should ideally measure axial thrust directly. However, friction, tautness of the feed tubes and other binding forces impact the measured force, hence the data reduction for actual thrust is not straightforward. A set of convergent (ASME) nozzles are used for checkout and calibration of the apparatus, as explained in section 2.2.

The flow from the floating plenum passes through two 30-mesh screens and then exhausts through the nozzle. The internal diameter of the floating plenum is 5" while the equivalent diameter of the nozzle exit is typically 1.3"; thus, the flow goes through a contraction ratio of about 15. This together with the two screens yields a uniform flow at the exit that was checked by Pitot surveys for an ASME 1.3" diameter nozzle.

The plug nozzle is attached to the end of the floating plenum (Fig. 1a). The nozzle (cowl) has a 2" exit diameter. There is a fixed 0.75" diameter stem held centrally within the nozzle by X-shaped struts; the geometry is the same as that used with the convergent cowl in [2]. A lead screw fixed to the stem is used to attach the interchangeable plugs. A few plugs are shown in Figs. 1(b-d). Three conic plugs with half angles of 10°, 16° and 22° (denoted as 'P10', 'P16' and 'P22') are shown in Fig. 1(b). Whereas the plugs in Fig. 1(b) are solid, corresponding porous plugs (denoted as 'PRS6', 'PRS2' and 'PRS7', respectively) are shown in Fig. 1(c). A porous plug has identical external geometry as its solid counterpart but has an internal cavity. The cavity has four quadrants separated by X-shaped struts to support the skin with pores. Some details of the 10° conic porous plug (PRS6) can be seen in the CAD drawings in Fig. 1(e). The pore diameter is 0.037" and the 'openness ratio', i.e., the ratio of open area due to the pores to the total surface area of the skin is 6% unless stated otherwise.

The three plugs shown in Fig. 1(d) were designed by a numerical optimization study [9]. The plug geometry was varied by varying three parameters, L_{t1}, L and P, as shown in Fig. 2(a); P is a measure of the roundedness of the contour, [9]. By varying these parameters, a wide range of plug geometries could be obtained.

Numerical simulation provided thrust coefficient for each geometry for varying NPR. A design space was queried to determine the geometry yielding optimum thrust at a chosen flight condition (NPR). This way, two optimum geometries were obtained for LTO and cruise conditions. These two are 'P38' and 'P39' in Fig. 1(d) and Fig. 2(b) (referred to as 'K1b' and 'K7' in [9]). Thus, P38 has the best *CFG* at LTO condition (NPR≈2) but lower *CFG* at cruise (NPR≈5.9), and vice versa for P39. The third geometry ('P40'; referred to as 'K9' in [9]) is a 'compromise' case yielding reasonably high *CFG* over the entire NPR range. Note that while MoC design for a convergent cowl yields a concave plug contour ('pear' shape), here for the cylindrical cowl the optimum plug contour turns out to be convex ('bulged' shape).

Spacers placed on the internal lead screw allowed for variation of the axial location of the plug relative to the nozzle exit. Also, the cylindrical section near the exit of the nozzle could be extended using lip extension pieces shown in Fig. 1(f). The extension pieces E1, E2, E3 and E4 simply fit over the end of the nozzle to extend the lip location by 0", 0.38", 0.74" and 1.34", respectively.

Overhead microphones were used for measurement of radiated noise. Noise data presented in this paper pertain to a nominal microphone location of 90° to the jet axis, 45" away from the jet exit. The microphone data acquisition is done using National Instruments A/D card and LabVIEW™ software. Sound pressure level spectral analysis is performed over 0-50kHz with a bandwidth of 50 Hz, using a data rate of 100 kHz and a 50 kHz low-pass filter. The 'jet Mach number' M_J is defined based on the plenum pressure, p_0, and the ambient pressure, p_a, and given by, $M_J = (((p_0 / p_a)^{(\gamma-1)/\gamma} - 1)\frac{2}{\gamma-1})^{1/2}$, where γ is the ratio of specific heats for air. The nozzle pressure ratio, NPR = p_0/p_a, and M_J are uniquely related to each other. These two parameters will be used interchangeably; values of both will be quoted in most cases. All data are for unheated flow, i.e., with the total temperature the same everywhere as in the ambient.

2.2 Data reduction for CFG

The performance of the thrust rig was assessed using convergent nozzles of different diameters. These nozzles have internal contours similar to standard ASME nozzles; the actual geometry can be seen in a later figure (and also in [2]). The measured axial force (*Tm*) and mass flow rate (*mdot*), for three such nozzles with exit diameters of 1.1", 1.3" and 1.5", are shown in Fig. 3(a) and (b) as a function of NPR; the NPR range of 1 - 5 corresponds to the M_J range of 0 - 1.71. Data for *mdot* are obtained by an orifice-meter in the supply line. The *Tm* data are compared in Fig. 4(a) with the calculated actual thrust (*Tac*) which is obtained as follows. The ideal thrust T_{ideal} is calculated first. This is simply a function of NPR (Eq. 4.33, [10]). It assumes uniform flow with zero boundary layer thickness. In the supersonic regime it represents the thrust had the flow expanded fully. A correlation for thrust coefficient (*CT*) for ASME nozzles, based on a large set of data, is given in [11]. This is used to determine $Tac=T_{ideal}*CT$. The force *Tac* would be measured had the thrust rig responded correctly. As it can be seen in Fig. 4(a) the measured force *Tm* differs from *Tac* due to various binding forces.

The binding forces due to tautness of the feed tubes under pressure was measured by capping the nozzle; this is denoted as *Tare*. The *Tare* data are also shown in Fig. 4(a). The expectation was that a correction with *Tare* would directly provide the actual thrust, i.e., *Tac* = *Tm*+*Tare*. However, for all conditions the measured *Tare* was not adequate to account for the difference between *Tm* and *Tac*. Furthermore, there was a small but perceptible hysteresis in *Tare* that can be seen in Fig. 4(a). The hysteresis could not be eliminated. At this point, the idea of measuring thrust directly was abandoned and an alternate method was adopted based on calibration data from the ASME nozzles.

The alternate method involved recording the difference *Tac-Tm* as a function of NPR for the ASME nozzles, as shown in Fig. 4(b). Now, for a plug nozzle *Tm* and *mdot* were measured as a function of NPR. For a given NPR, the *mdot* data was used to find an equivalent diameter (D_{eq}) by interpolation of the calibration data of Fig. 3(b). The value of $\triangle T = Tac - Tm$, for that D_{eq} and NPR, was then found from Fig. 4(b). This yielded the expected actual thrust, $Tac = Tm + \triangle T$. Calculated ideal thrust provided the gross thrust coefficient as defined by, $CFG = Tac/T_{ideal}$. The uncertainty in the *CFG* data obtained over a period of weeks was large. However, it was small enough for data obtained back-to-back to allow an assessment of comparative performance with parametric variations. The repeatability of *CFG* (as measured by its standard deviation) for several sets of data for the 1.3" ASME nozzle, acquired over a day, was 0.45% and 0.7% for NPR of 4.2 and 2, respectively. Thus, while the absolute amplitudes were not reliable the relative amplitudes for parametric variation with data taken back-to-back should be representative.

In the following, noise data followed by schlieren pictures for parametric variation are discussed first. The effects of plug shape and porous plugs are documented. In particular, the occurrence of various deleterious noise components, namely, screech tones, broadband shock associated noise (BBSN), transonic tones and excess broadband noise (EBBN), and the effect of plug porosity on them are examined. Finally, limited thrust data are discussed with corresponding numerical simulation results.

3. Results

3.1 Plug shape and crown location effect on noise and flow field

Sound pressure level (SPL) spectral data for the three optimized plugs, P38, P39 and P40 are presented in Fig. 5. Data for two nominal jet Mach numbers of 1.00 and 1.64 are shown. Recall that plugs P38 and P39 represent optimum geometries for LTO and cruise conditions, respectively, while plug P40 is a compromise case. The data in Fig. 5(a) represents a LTO condition. The crown location $\triangle x$, M_J and OASPL (dB) are shown in the 2nd, 3rd and 4th columns of the legend, respectively, in this and all subsequent spectral figures. For all data in Fig. 5 the crown location is near the exit ($\triangle x$= -0.035") which is the design location for the P38 plug at LTO condition. Clearly, P39, designed for cruise with design $\triangle x$ smaller than -0.035, is noisier in Fig. 5(a). The noise data at the higher M_J in Fig. 5(b), for P39 and P40 with the given $\triangle x$, may not have an application significance since those plugs would be drawn inside the cowl to achieve appropriate throat-to-exit area ratio for flow expansion. Nonetheless, those data are included to provide a broad perspective of the noise generated by these plugs. In Fig. 5(b), BBSN, represented by the broad peak around 4.5kHz, dominates the spectra for all plugs. This peak is seen to be most pronounced for the P39 case and least for the P40 case. Later, it will be seen that BBSN as well as screech tones can occur with all three plugs even when they are placed inside the cowl.

Schlieren data corresponding to the cases of Fig. 5 are shown in Fig. 6. These are instantaneous pictures, and data for M_J =1 (NPR=1.89) and M_J =1.67 (NPR=4.75) are shown in the upper and lower rows, respectively. (The highest available M_J varied somewhat from day to day depending on the ambient pressure. This accounts for variation in the higher M_J in some of the figures). Shocks can be seen just past the nozzle exit at M_J =1, as the flow accelerates around the plug crown. The shock is least pronounced for the P38 case which has a mild curvature around the crown. At the higher M_J, all three plugs exhibit a bulging flow out of the nozzle representing underexpanded condition. This is expected since with the crown located near the nozzle exit the flow passage is essentially convergent.

For a given plug, the crown location ($\triangle x$) determines the throat-to-exit area ratio. Within the experimental constraints the crown location could be varied in discrete steps. The approximate values of $\triangle x$ for obtaining throat-to-exit area ratios for optimum thrust at NPR of 4.61 (M_J =1.65) are $\triangle x$= -0.9", -0.415" and -0.415" for

the P38, P39 and P40 cases, respectively. Noise and schlieren data were acquired for the three plugs with those respective locations and shown in Figs. 7 and 8, at M_J =1.65 as well as at M_J =1.55 with the same △x. It is seen that the LTO optimized plug (P38) is still least noisy (Fig. 7, red traces). P39, designed for NPR=5.9 (M_J =1.82), is seen to produce the highest BBSN peak as well as a screech component (blue traces). The compromise case (P40, green) has an intermediate level of noise. Schlieren data in Fig. 8, corresponding to the conditions of Fig. 7, exhibit shock structures that are similar for all three plugs. At M_J =1.65 all flows appear somewhat overexpanded as evident from the inward trajectory of the jet boundary. The shock boundaries appear sharper for the P39 case indicating stronger shocks commensurate with higher levels of shock-associated noise (BBSN and screech).

The relative crown location effect is studied with the 16° conic plug. A 16° conic plug has been used in a larger-scale NASA experiment in the past [10, 11], and is to be used in another upcoming experiment. Thus, noise and schlieren data for this plug with varying △x could be useful. Numerical simulations are also performed with this plug and comparison with experimental thrust data will be discussed in section 3.3. SPL spectra for the P16 plug are shown for four crown locations of -0.286", -0.665", -1.025" and -1.625", for M_J =1.05 (NPR =2, LTO) and M_J =1.65 (NPR=4.61, cruise) in Figs. 9(a) and (b), respectively. The crown locations were achieved simply using the four extensions E1, E2, E3 and E4 without any spacers. The spectral data are staggered for clarity; successive traces are shifted by 5 dB, the ordinate being pertinent to the trace at the bottom. First, at the higher M_J in Fig. 9(b) BBSN peak and screech tones are seen. The frequencies of the BBSN peak do not change significantly with varying △x. Perhaps, this is expected since BBSN (as well as screech) depend on the shock structure outside the nozzle that does not change significantly with △x (see schlieren data next). In Fig. 9(a), at M_J =1.05 (NPR=2), a large spectral peak representing a loud tone occurs for the upstream-most crown location (△x =-1.625"). This is a transonic tone discussed shortly.

Schlieren pictures corresponding to the conditions of Fig. 9 are shown in Fig. 10. At the higher M_J of 1.65, the shock structure appears weak for the upstream-most crown location (bottom right). This is expected as with that crown location the throat-to-exit area ratio approaches the design value for full expansion. At the lower M_J of 1.0 and △x= -1.625" (bottom left), the condition of transonic tone, the flow exhibits organized large-scale vortical structures. Such structures are visible randomly in the instantaneous pictures. (No attempt was made to obtain phase-locked pictures at this time.)

3.2 Plug porosity effect

The effect of plug porosity on noise and flow is now addressed. Data for the 10° conic plug, as shown in Figs. 11 and 12, exhibit a profound effect. Pairs of spectral data are presented in Fig. 11, for the solid (P10) and the corresponding porous plug (PRS6), for four values of M_J all with △x= -0.035". Significant effects are noticed at the jet Mach numbers covered. BBSN and screech are effectively suppressed by the porosity. (At lower M_J and subsonic conditions practically no effect was observed, data not shown for brevity).

Corresponding schlieren data are shown in Fig. 12. A comparison of the images shows that the shock structure occurring with the solid plug (for example, at M_J =1.4) has weakened by the porosity. Similar data with the convergent cowl at same M_J exhibited a more pronounced effect [2], exhibiting a drastic weakening and splintering of the shocks; the reduction of the BBSN peak in noise spectra was also more dramatic. Between the earlier and the present experiments significant changes in the facility took place due to installation of the thrust apparatus. However, the earlier cowl with the same plugs were re-examined in the current facility setup, and the previous noise as well as schlieren data repeated well. Thus, the noted differences must be due to cowl geometry. With the cylindrical cowl the plug porosity effect is not as pronounced. Nonetheless, the noise suppression is very significant as seen in Fig. 11.

It was anticipated that the 16° conic plug would also exhibit a similar effect of porosity on noise. This would allow an advocacy for including a porous plug in the upcoming larger-scale NASA experiment that will employ a similar plug. A 16° plug, which is shorter and lighter than the 10° plug, is preferable from an application point of view. Unfortunately, the porosity effect with the 16° case was minimal, in fact, an increase in noise occurred under certain conditions. The noise data shown in Fig. 13, illustrates this. Note the appearance of BBSN and screech for the porous case in Fig. 13(c) that was absent with the solid case. Corresponding schlieren data presented in Fig. 14 do not seem to shed light on these conflicting effects and the underlying mechanisms for the observed trends remain unclear at this time. We note here that data taken with the 22° conic case (not shown for brevity) also exhibited no significant effect of the porosity. Repeat measurements with the 10° case, on the other hand, exhibited the suppression of BBSN and screech as seen in Fig. 11 consistently. Thus, a longer plug may be needed to realize the beneficial effect of porosity on noise. Preliminary thrust data also show a better thrust performance for the 10° plug relative to the shorter plugs, as well as minimal thrust loss due to the porosity, discussed shortly.

Transonic tone and EBBN: Recall the Transonic tone observed in Fig. 9. The characteristics of these 'x-tones' and the related phenomenon of excess broadband noise (EBBN), occurring with plug nozzle flows, is explored using the 10° conic plug. The x-tone phenomenon, studied in [12], occurs with convergent-divergent nozzles when a shock resides within the divergent section. The unsteady shock motion locks on to one-quarter wave acoustic modes of the divergent section to produce the intense tone. Later it was found that even in the absence of a locked-in resonance, the broadband noise levels are unusually high relative to the noise from a convergent nozzle of same throat (or exit) area at same NPR. The high noise was termed excess broadband noise and attributed to unsteady shock motion within the divergent section that is random (not periodic due to lock-in with any acoustic mode); [13]. The same phenomena occur with a plug nozzle flow, when the plug crown is inside the cowl creating a convergent-divergent passage.

SPL spectra are shown in Fig. 15(a) for a number of M_J for the 10° conic plug placed with $\triangle$x= -1.625". For clarity the data are shown in a staggered pattern, similarly as in Fig. 9. It can be seen that with increasing M_J a tone occurs around M_J =0.53; the frequency increases with increasing M_J and then goes through a stage jump around M_J =0.86; eventually the tone ceases for M_J >1.04 for the given configuration. The frequency of the spectral peak (in kHz) and its amplitude (in dB, with the given analysis bandwidth) are shown in Fig. 15(b). The stage on the right in Fig. 15(b) is recognized as the fundamental ¼-wave resonance, hence it is denoted 'stage 1'; 'stage 2' represents the third harmonic. A curious reader may find further details in [12].

The straight lines through the frequency data in Fig. 15(b) are from a correlation equation provided in [12]. In the correlation, the tone frequency, nondimensionalized by the velocity and the throat-to-exit length, is expressed as a function of the half-angle of the divergent section. For the present case an equivalent half-angle is calculated from the throat and exit areas to be 7.94°. There is some ambiguity regarding the length scale. The average distance of two points on the plug surface, measured from the throat, is taken as the length scale. One of these points is at the intersection of the nozzle exit plane with the plug (1.625"), and the other is the intersection of a line drawn from the nozzle lip and perpendicular to the plug surface (1.449"). Thus, the length scale is taken as 1.537". Note that the correlation is based on data from various convergent-divergent nozzles. The plug nozzle has an annular flow and thus some differences may be expected. Nonetheless it is seen that the correlation agrees reasonably well with the frequency data leaving no doubt that the tone observed here is the same as the transonic tone.

It should be noted here that with increasing M_J (and NPR) the threshold at which the throat becomes choked depends on the throat-to-exit area ratio. The smaller is this ratio the lower is the threshold. In the present case (equivalent diameters of throat and exit being 1.276" and 1.732") the threshold is at about M_J =0.336 (NPR =

1.081). Note that there is a range of M_J between the x-tone stages (Fig. 15) when there is no tone. There are also methods that eliminate x-tones [12]. However, in all cases in the absence of any tone, it was shown in [12] that the broadband noise levels were high relative to what is expected from a convergent nozzle of same throat area at same NPR. For the plug nozzles, this is examined further in the context of plug porosity effect.

Plug porosity effect on transonic tone and EBBN: SPL spectra for the 10° plug are presented in Fig. 16 for solid (P10, red lines) and porous (PRS6, blue lines) cases, at four M_J with △x=-1.625". Figure 16(a) and (b) captures the x-tone in the two stages, seen in Fig. 15 (for the solid plug). It is readily seen that the porosity completely eliminates the x-tone. Figure 16(c) shows spectra at a condition between the two x-tone stages (Fig. 15) where there is no tone. It is instructive to first compare the data for the solid plug (red line) with that from a simple convergent nozzle (grey line), that has the same exit area as the throat of the plug nozzle (1.3" diameter). The red line is 6-8 dB higher in amplitude; this difference is EBBN. Now note the effect of the porous plug; it has suppressed the EBBN and brought the levels down significantly reducing OASPL by 5.5dB. Figure 16(d) is included to show the suppression of EBBN for a different crown location of △x=-1.025"; here, OASPL has reduced by about 5dB. Schlieren pictures for the three △x=-1.625" cases are shown in Fig. 17. Large scale vortical structures are visible with x-tone (see the top two pictures on left column) as well as the case of EBBN (the bottom picture on left column). The porous plug has weakened the vortical structures leading to the suppression of the aberrant noise components. The effect likely traces to a weakening of the shock(s) by porosity within the divergent section.

As indicated before, certain methods e.g., tripping the boundary layer near the throat was successful in suppressing x-tones [12]. However, no method had been known for suppression of EBBN. Similarly, with reference to the data in Fig. 11, there are known methods for suppression of screech tones (such as by placing a tab at the nozzle lip) but none that would suppress BBSN. The porous plug has suppressed both EBBN and BBSN in addition to eliminating screech and x-tone. It is plausible that a porous plug with a fixed crown location inside the cowl may serve to produce low noise at LTO while yielding optimum thrust at cruise. Such a fixed porous plug, providing good thrust throughout the entire flight range and low noise at LTO, would obviously be desirable rather than a translating plug requiring different crown position in different flight regime. This would simplify the design as well as reduce weight. Such a possibility, however, will require more research numerically as well as experimentally. Once again, we note that the porosity effect on noise suppression occurred only with the longer 10° plug. Unfortunately, it does not seem to occur with the shorter porous plugs that would have been even more desirable from an implementation point of view.

3.3 Thrust data compared to CFD results:

Limited thrust data are now presented with accompanying Computational Fluid Dynamics (CFD) analysis. The CFD calculations are performed using ANSYS Fluent software, assuming axisymmetric steady state and fully turbulent compressible flow of calorically perfect air, with Reynolds-averaged Navier-Stokes model equations solved implicitly over adaptively refined unstructured meshes. Further details of the CFD analysis can be found in [9]. First, as a sanity check, *CFG*, defined in section 2.2, for the *D*=1.3" ASME nozzle is examined in Fig. 18. Experimental data and CFD data are shown by the red (solid) and the blue (dashed) curves, respectively. The trends and the amplitudes agree well, considering the uncertainties in the experiment as well as in the simulation.

The results in Fig. 18(a) are also compared with analytical predictions. The ratio T_{conv}/T_{ideal} is shown by the green line; T_{conv} is the calculated thrust for a convergent nozzle. Both T_{ideal} and T_{conv} assume top-hat exit velocity profile with zero boundary layer thickness. Whereas T_{ideal} assumes full expansion of the flow T_{conv} accounts for the unbalanced pressure at the nozzle exit, in supersonic conditions. The ratio is unity in subsonic conditions (NPR < 1.89) and it decreases with increasing NPR in supersonic conditions. The solid light blue

curve is the correlation *CT* for ASME nozzles from Ref. [11]; recall discussions in section 2.2 that $CT=Tac/T_{ideal}$. Its difference from the green curve is primarily due to boundary layer losses. Ideally, the experimental and CFD results should agree with the light blue (*CT*) curve. Observed differences are not unexpected. Apart from data uncertainty there can be differences in the boundary layer states. (There is considerable scatter in the data from which the correlation equations were derived in [11]). Thus, the agreement with the predictions is considered reasonable and these results, in fact, provided confidence in the present methods. The plot in Fig. 18(b) is a sample CFD data clip at NPR=4.25; calculated flow fields like this yielded the *CFG* results shown in Fig. 18(a). Figure 18(b) also shows the geometry of the *D*=1.3" ASME nozzle.

Figure 19 shows experimental thrust results compared to CFD results corresponding to the 16° conic plug data shown in Figs. 9 and 10. The effect of four axial locations of the plug crown on *CFG* is shown as a function of NPR. In the sketch in Fig. 19(b), the extension E1 ($\triangle$x= -0.035") is represented by the dark blue wall; lip locations for extensions E2, E3 and E4 ($\triangle$x= -0.665", -1.025" and -1.625")) are shown by the red, green, and grey walls, respectively. The same color code is used for the data in Fig. 19(a), where the solid lines represent experimental data, and the dashed lines represent CFD results. It is seen that the data trends as well as amplitudes agree reasonably well between the experiment and CFD. These results provided added confidence in the adopted CFD procedure.

Finally, the plug porosity effect on *CFG* is illustrated in Fig. 20, with experimental data for the 16° and 10° conic plugs and their porous counterparts. The same scales as in Fig. 19(a) are used for comparison. While a reduction in *CFG*, due to porosity, in the order of 1% is noted for the 16° case (Fig. 20a), a smaller reduction over most of the NPR range is noted for the 10° case (Fig. 20b). These results delineate that the losses in *CFG* with the presently used porous plugs are small. We have seen that the noise reductions by the 10° conic porous plug was quite significant. It suppressed not only screech tones and x-tones but also BBSN and EBBN, with less than 1% loss in *CFG*.

Conclusions

A fundamental study was carried out with the aim of providing recommendations for the best external plug geometries for supersonic aircraft concepts in an ongoing NASA program. To that end, numerical optimization studies provided optimum plug geometries for LTO and cruise conditions. With a cylindrical cowl these shapes turned out to be characterized by convex contours or bulges. Such shapes differ from the pear-like plug shapes with concave contours as predicted by method of characteristics for convergent cowls, which have been used practically in all previous plug nozzle studies. The LTO and cruise conditions yielded largely different plug shapes; a compromise shape was also developed with the hope that it would provide adequate performance over the full operating range. These three plug shapes were explored in the present experimental study, in addition to conic shaped plugs as well as porous plugs. Noise and flow field data were examined over a range of NPR up to about 4.7. An emphasis was to look for geometries that would yield minimum noise at low NPR (LTO) while not sacrificing thrust at cruise.

Results show that a plug designed for optimum thrust at cruise was noisier throughout the NPR range covered. A plug designed for optimum thrust at LTO had lower noise throughout the NPR range while the compromise plug case had intermediate noise levels. The results also show that a plug nozzle, depending on its crown location relative to the nozzle exit, could generate transonic tones (x-tones) and excess broadband noise (EBBN) at low NPR, apart from the well-known screech tones and broadband shock associated noise (BBSN) at high NPR. A long porous plug was found to effectively suppress all these aberrant noise components while suffering less than 1% loss in thrust coefficient. Future efforts will aim at optimization of the porous plug geometry for maximum suppression of LTO noise while minimizing thrust loss.

Thrust coefficient data acquired for a few cases showed good agreement with corresponding numerical simulation results. This provided confidence in the numerical methods that will be used to investigate the extensive parameter space for optimizing the plug geometry. At present the experimental data on thrust coefficient has significant uncertainties. Efforts are under way to improve the thrust measurement apparatus, which will not only benefit future experiments with plug nozzles but also other propulsion components.

Acknowledgement

The work is supported by NASA's Commercial Supersonic Technology (CST) Project under NASA's Advanced Air Vehicles Program.

References

1. Zaman, K.B.M.Q. and Heberling, B.C., 2021, "A study of flow and noise from supersonic plug nozzles", *AIAA Paper* 2021-2304, Aviation Forum, August 2-6, 2021.

2. Zaman, K.B.M.Q., Fagan, A.F. and Korth, J.H., 2024, "Flow and noise and thrust of supersonic plug nozzles", *AIAA Paper* 2024-2305, AIAA SciTech 2024 Forum, Orlando, FL., January 8-12, 2024.

3. Krull, H. G. and Beale, W. T., "Effect of Plug Design on Performance Characteristics of Convergent-Plug Exhaust Nozzles", *NACA RM* E54HO5, 1954.

4. Georgiadis, N.J., DalBello, T.W., Trefny, C.J., and Johns, A. L., "Aerodynamic Design and Analysis of High Performance Nozzles for Mach 4 Accelerator Vehicles", *AIAA Paper* 2006-16, 44th AIAA Aerospace Sciences Meeting and Exhibit, Reno, Nevada, 2006.

5. Angelino, G., "Approximate Method for Plug Nozzle Design", *AIAA J*., vol. 2 (no. 7), pp. 1834-1835, 1964.

6. Hagemann, G., Immich, H., and Terhardt, M., "Flow Phenomena in Advanced Rocket Nozzles – The Plug Nozzle," *AIAA Paper* 98-3522, 34th Joint Propulsion Conference and Exhibit, Cleveland, OH, July 1998.

7. Bridges, J.E., Podboy, G.G. and Wernet, M.P., "Plug20 Test Report", NASA TM 20210010291, 2021.

8. Bridges, J.E. and Wernet, M.P., "Noise of Internally Mixed Exhaust Systems With External Plug For Supersonic Transport Applications", AIAA Paper 2021-2218, Aviation Forum, August 2-6, 2021.

9. Korth, J.H., "Optimization of Plug Nozzles Using CFD Informed Design Space Querying", *AIAA Paper* 2024-1776, SciTech Conference, Orlando, FL, January 8-12, 2024.

10. Shapiro, A.H., "The dynamics and thermodynamics of compressible fluid flow, volume I", The Ronald Press Company, New York, USA, 1953.

11. Mikkelsen, K. L. and Brasket, R. G., "An Equation Set for ASME Nozzle Discharge and Thrust Coefficients," *AIAA Paper* 2011-1265, Jan. 2011.

12. Zaman, K.B.M.Q., Dahl, M.D., Bencic, T.J. and Loh, C.Y., "Investigation of a 'transonic resonance' with convergent-divergent nozzles", *J. Fluid Mech*., 463, pp. 313-343, 2002.

13. Zaman, K.B.M.Q., Bridges, J.E. and Brown, C.A., “Excess broadband noise observed with overexpanded jets”, *AIAA J.*, 48(1), pp202-214, 2010.

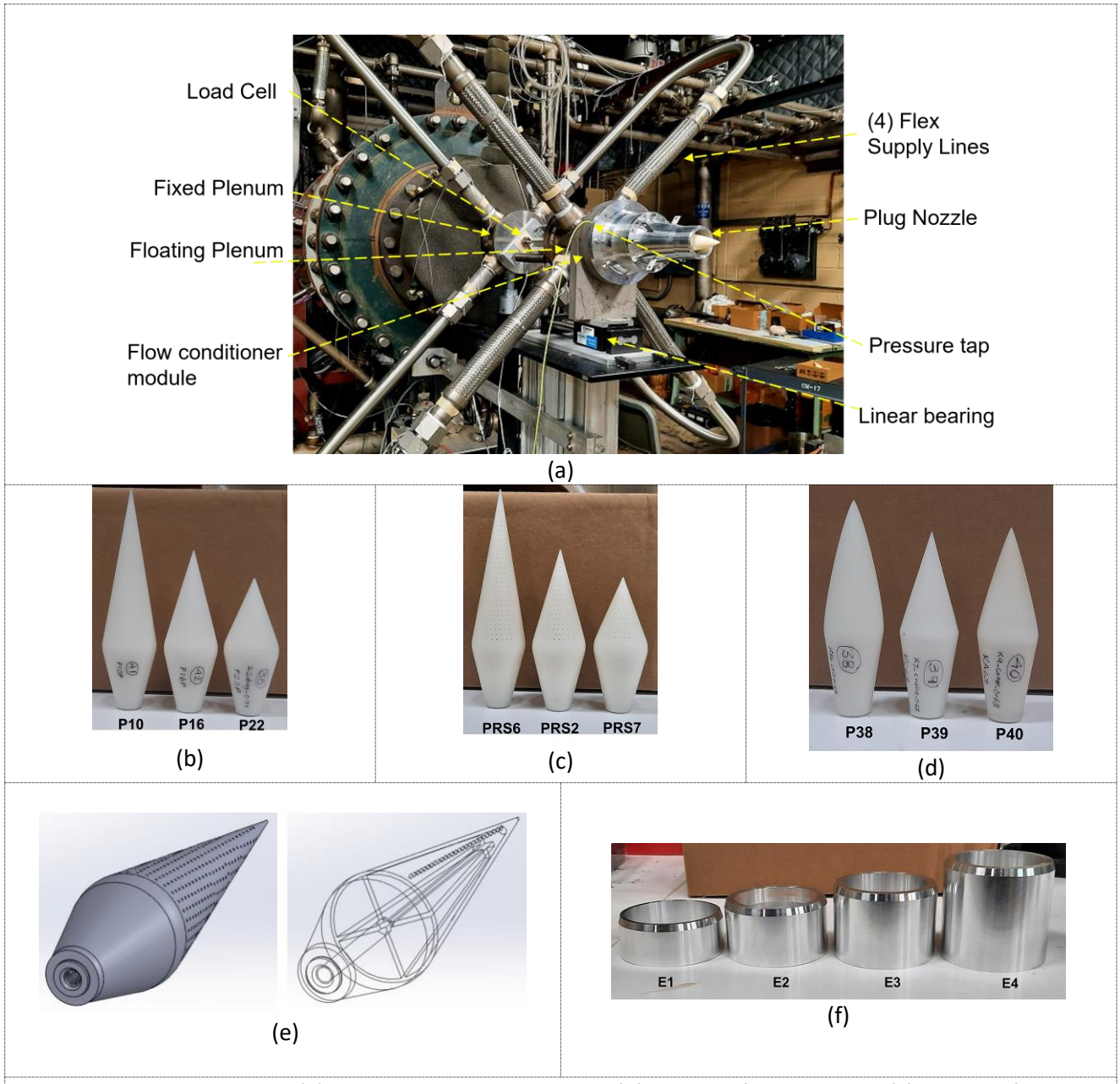

Fig. 1 Experimental Facility. (a) Thrust measurement setup, (b) picture of 3 solid plugs, (c) picture of 3 porous plugs, (d) optimized plugs via numerical study, (e) CAD drawing of a porous plug, (g) picture of nozzle lip extensions.

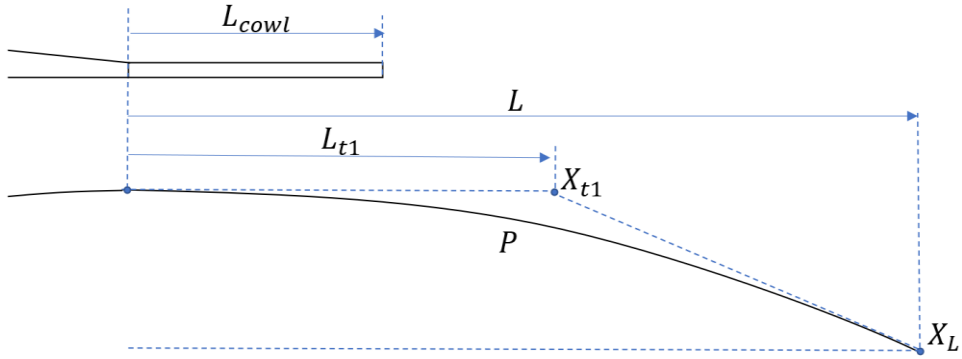

(a)

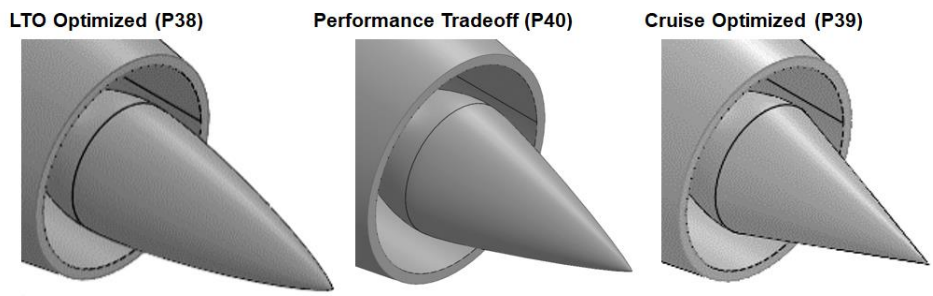

(b)

Fig. 2 Optimization of plug geometry via numerical simulation from [9]. (a) plug parameters varied for optimization, (b) Resultant plug geometries optimized for LTO (left) and cruise (right), as well as a 'compromise' geometry (middle).

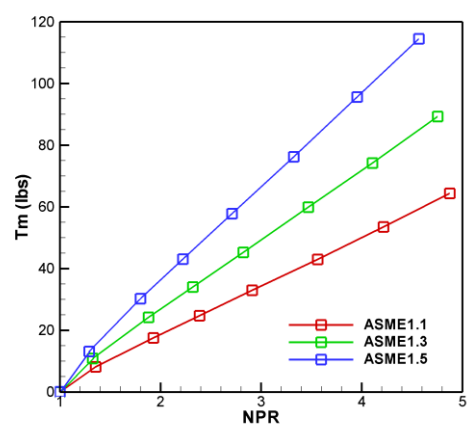

(a)

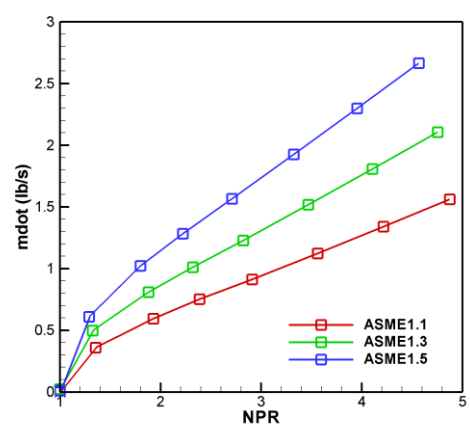

(b)

Fig. 3 Calibration data with three 'ASME' nozzles having diameters of 1.1", 1.3" and 1.5". (a) Measured axial force (*Tm*), (b) measured mass flow rate (*mdot*), as a function of NPR.

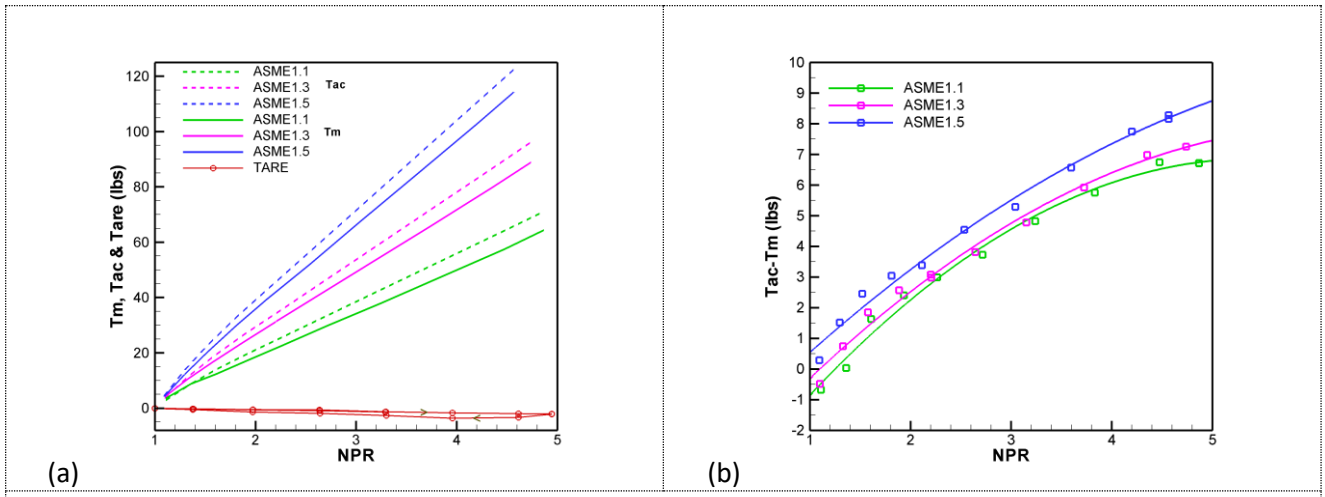

Fig. 4 Force data for three ASME nozzles. (a) Measured force (*Tm*) and calculated actual force (*Tac*) shown by solid and dashed lines, respectively; '*Tare*' force (red) for no-flow. (b) Difference (*Tac-Tm*) for the three nozzles.

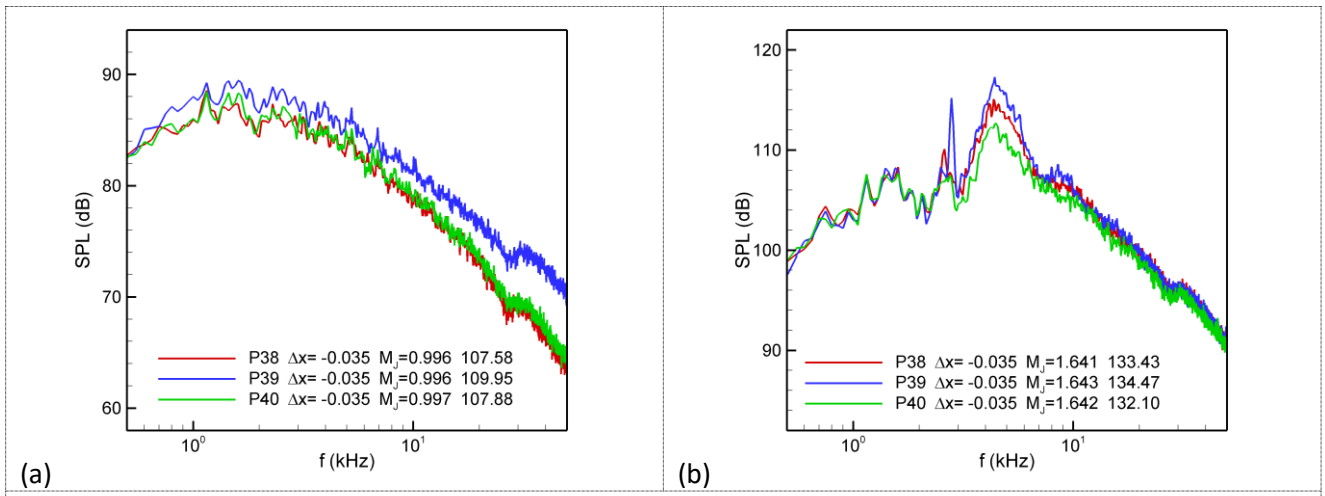

Fig. 5 Sound pressure level (SPL) spectra at θ≈90° for the three optimized plugs; crown location △x= -0.035". Plug case, crown location, jet Mach number and overall sound pressure level (OASPL, dB) are indicated in the legend. (a) M_J ≈1.0, NPR≈1.89, 'LTO' condition, (b) M_J ≈1.64, NPR≈4.61, 'cruise' condition.

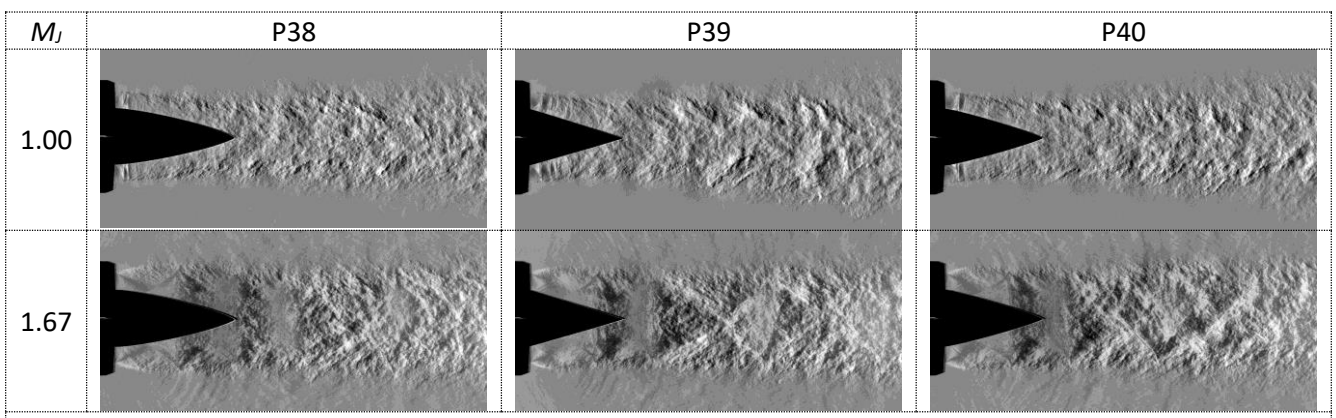

Fig. 6 Schlieren images of flows corresponding to the noise data in Fig. 5.

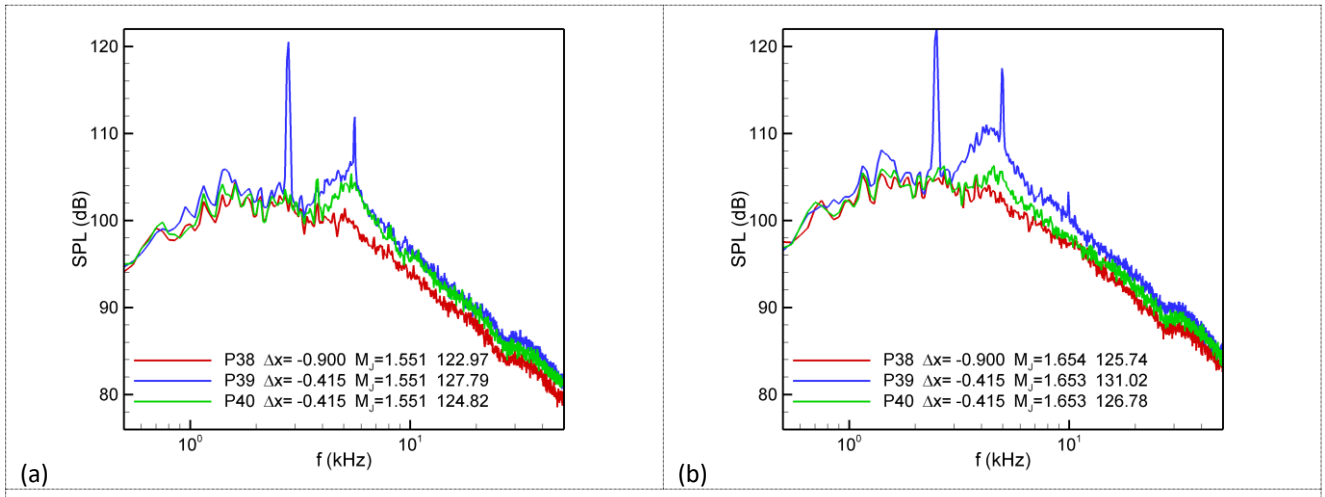

Fig. 7 SPL spectra at θ≈90° for the three optimized plugs: P38 with △x=-0.90” (red lines), P39 with △x=-0.415” (blue lines) and P40 with △x=-0.415” (green lines). Data shown for two M_J of 1.55 and 1.65 in (a) and (b).

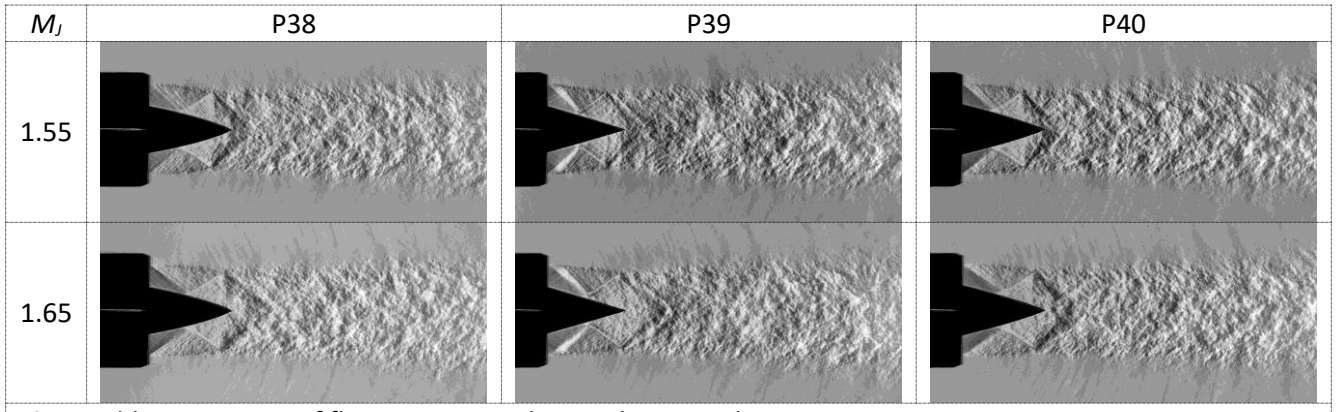

Fig. 8 Schlieren images of flows corresponding to the noise data in Fig. 7.

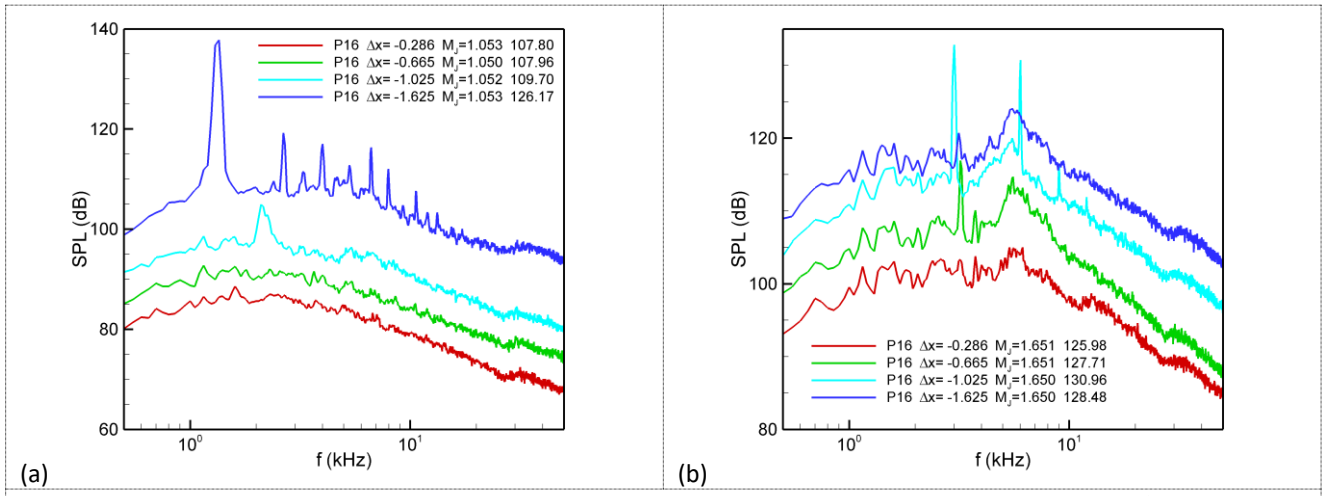

Fig. 9 SPL spectra for the 16° conic plug (P16) with different extensions (crown locations), E1 (△x=-0.285”), E2 (△x=-0.665”), E3 (△x=-1.025”) and E4 (△x=-1.625”). Successive traces are staggered by 5dB. (a) M_J =1.005 (NPR=1.9) and (b) M_J =1.65 (NPR=4.61).

Extension	M_J =1.005 (NPR=1.9)	M_J =1.650 (NPR=4.61)
E1 (△x=-0.285”)	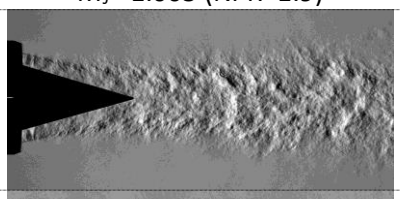	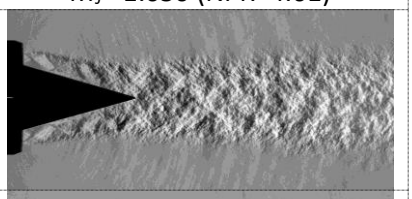
E2 (△x= -0.665”)	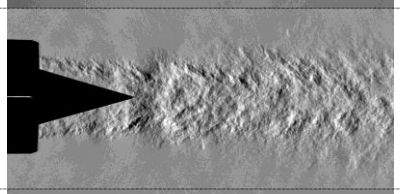	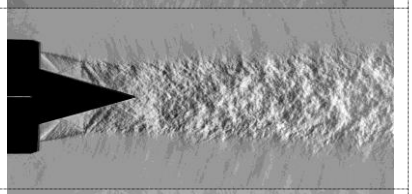
E3 (△x= -1.025”)	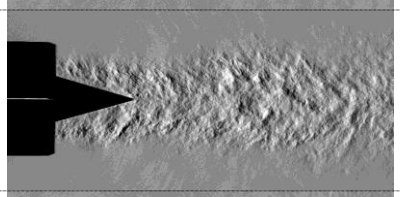	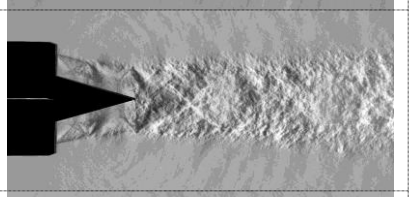
E4 (△x= -1.625”)	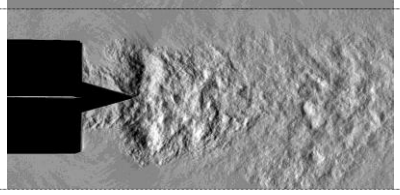	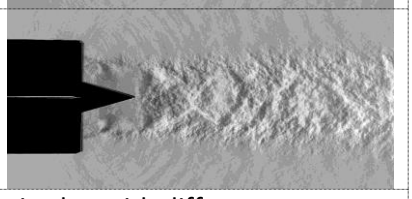

Fig. 10 Schlieren images of flows for the 16° conic plug with different extensions corresponding to the noise data of Fig. 9.

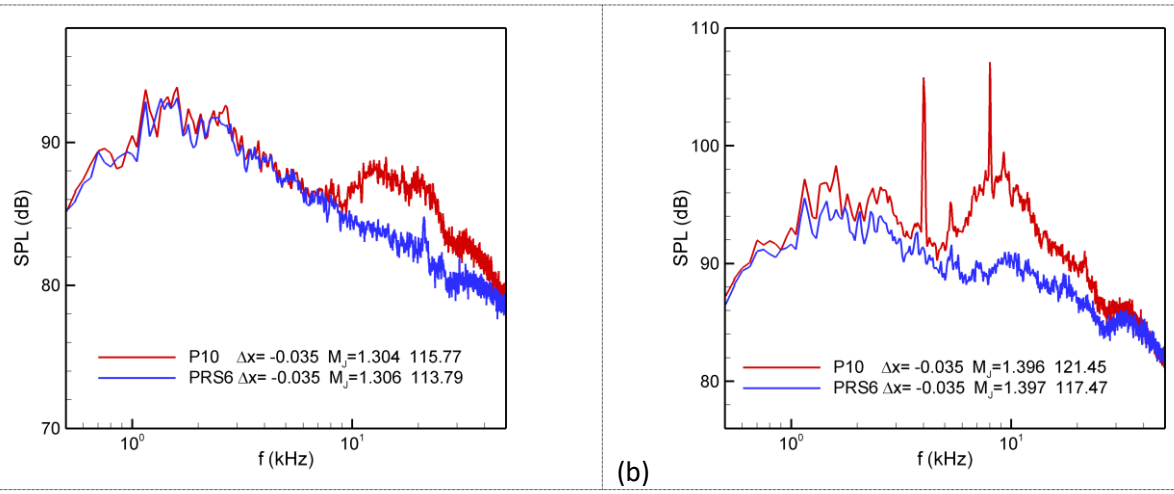

Fig. 11 Continued next page.

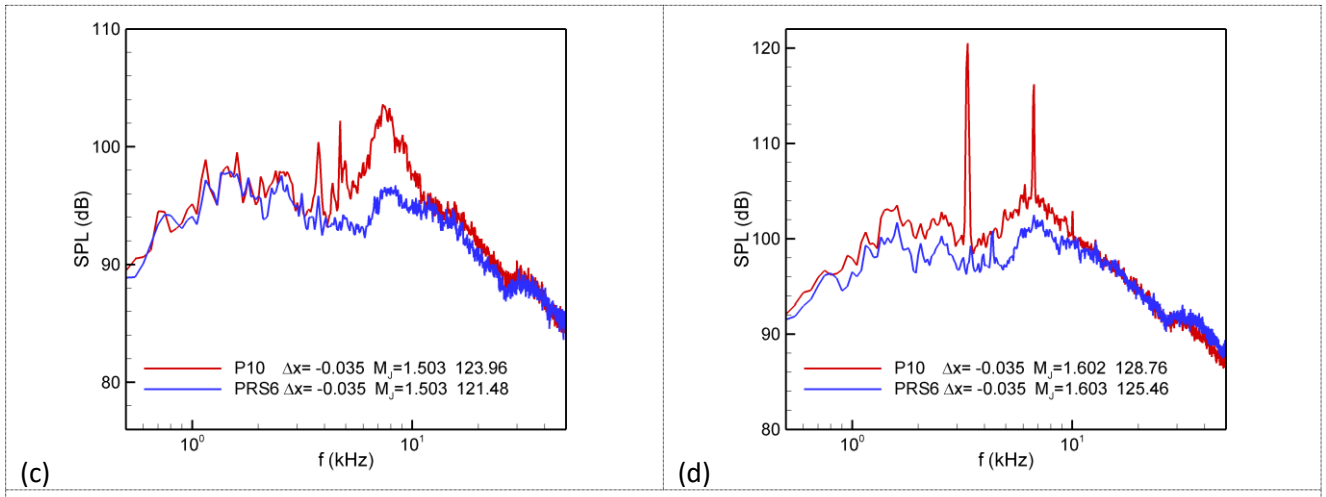

Fig. 11 SPL spectra at θ≈90° for the 10° conic plug showing plug porosity effect. Red lines: solid plug (P10), blue lines: porous plug (PRS6).

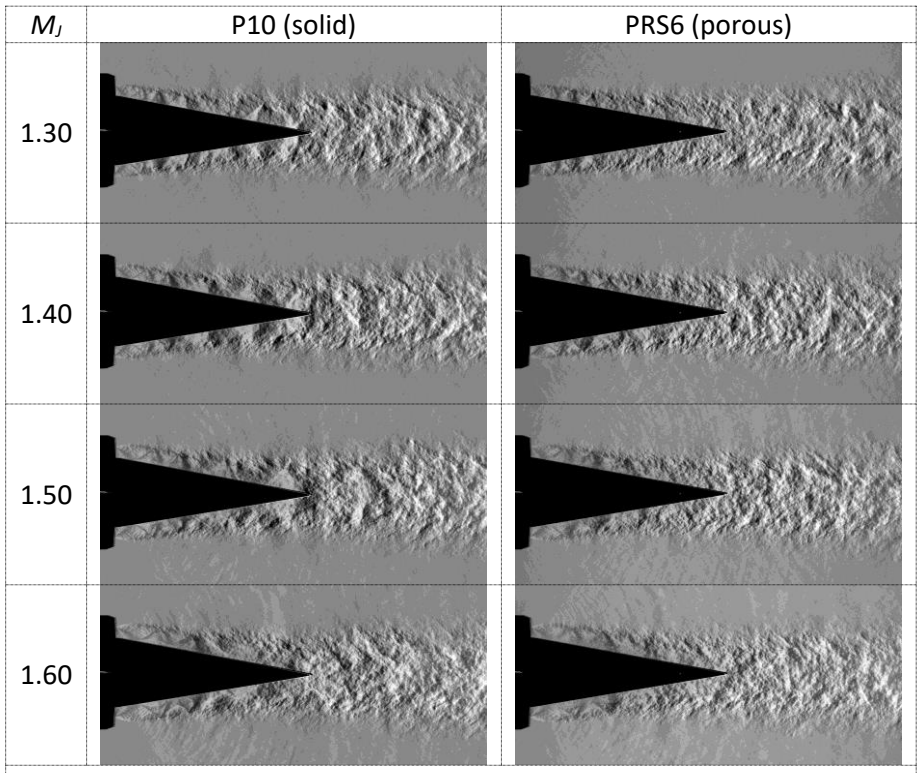

Fig. 12 Schlieren images of flows for the 10° conic plug corresponding to the noise data of Fig. 11.

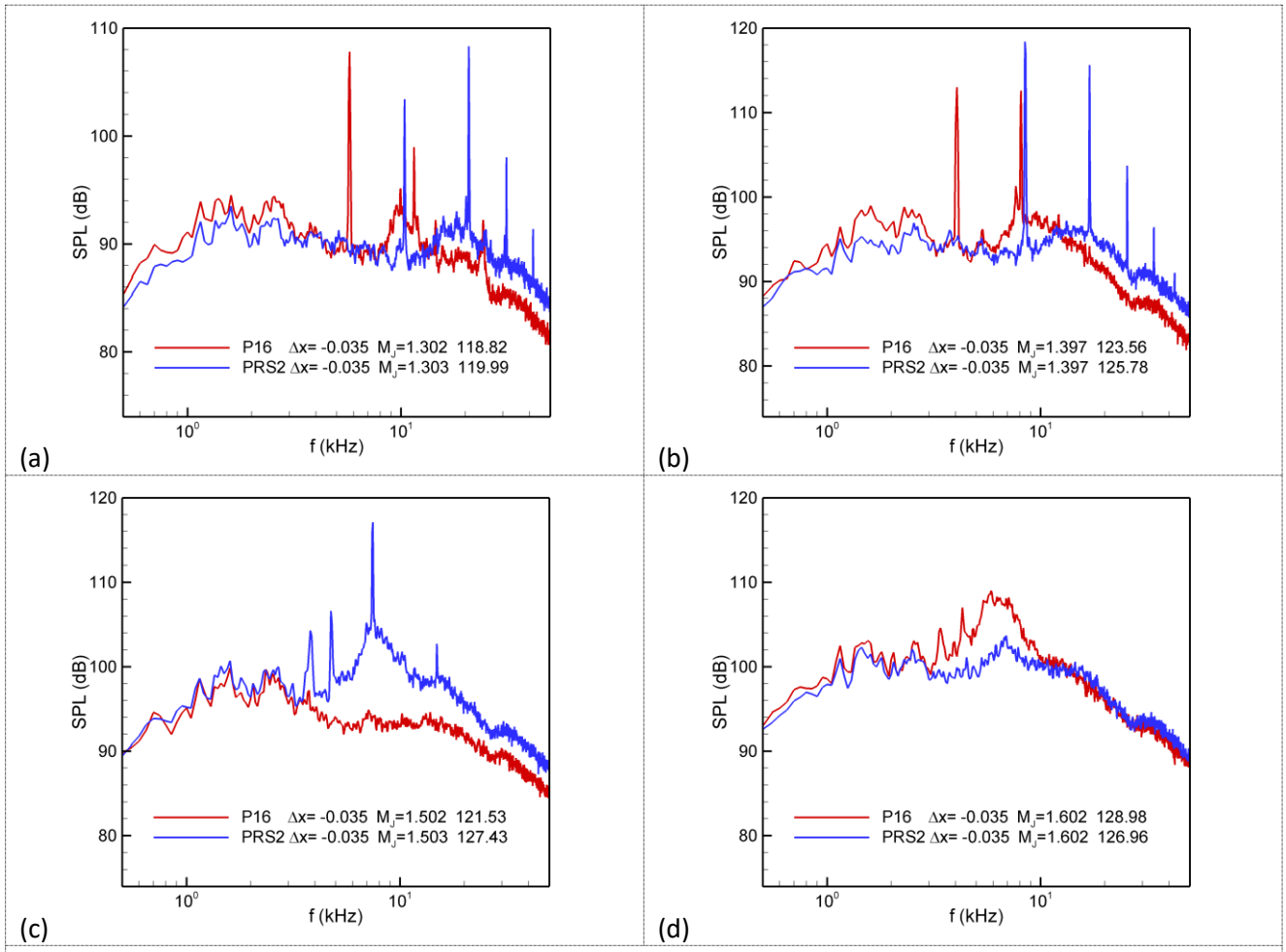

Fig. 13 SPL spectra at θ≈90° for the 16° conic plug showing plug porosity effect. Red lines: solid plug (P16), blue lines: porous plug (PRS2).

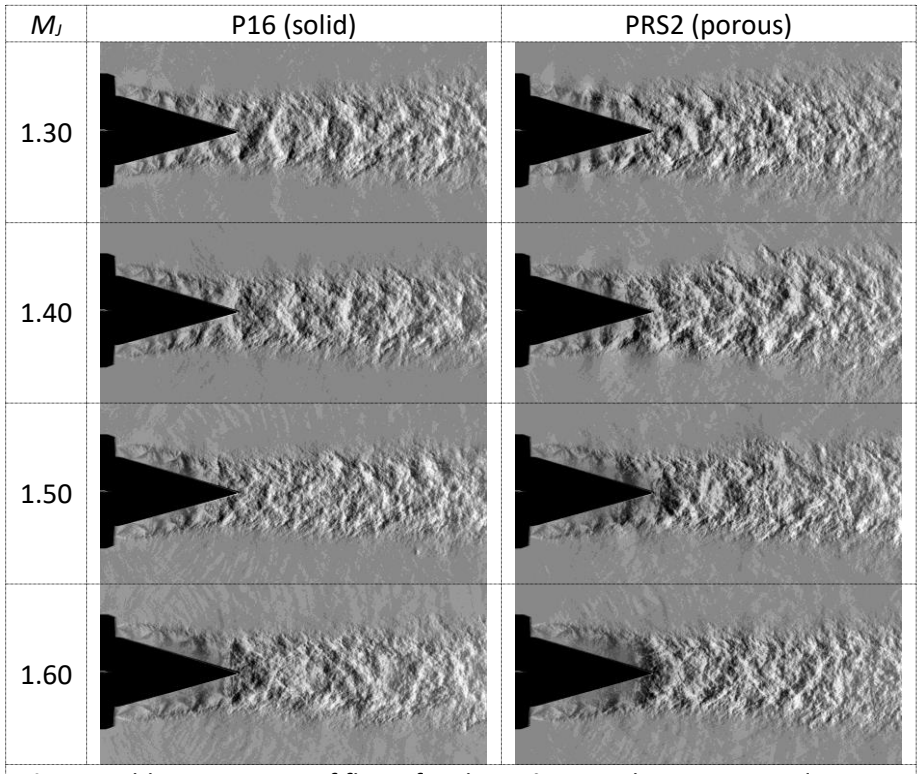

Fig. 14 Schlieren images of flows for the 16° conic plug corresponding to the noise data of Fig. 13.

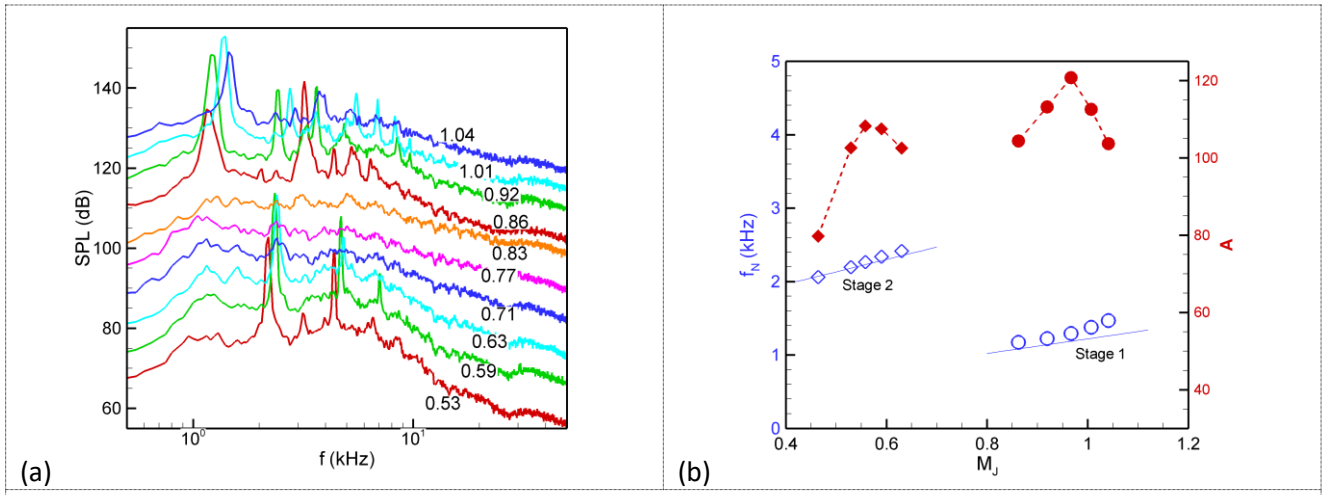

Fig. 15 Characteristics of x-tone for the 10° conic plug (P10) with crown location, △x=-1.625”. (a) SPL spectra at various M_J (successive traces staggered by 5dB, ordinate pertains to trace at bottom), (b) x-tone spectral peak frequency and amplitude as a function of M_J, solid lines prediction by correlation given in [12]; M_J range 0.4-1.2 corresponds to NPR range of 1.12-2.42.

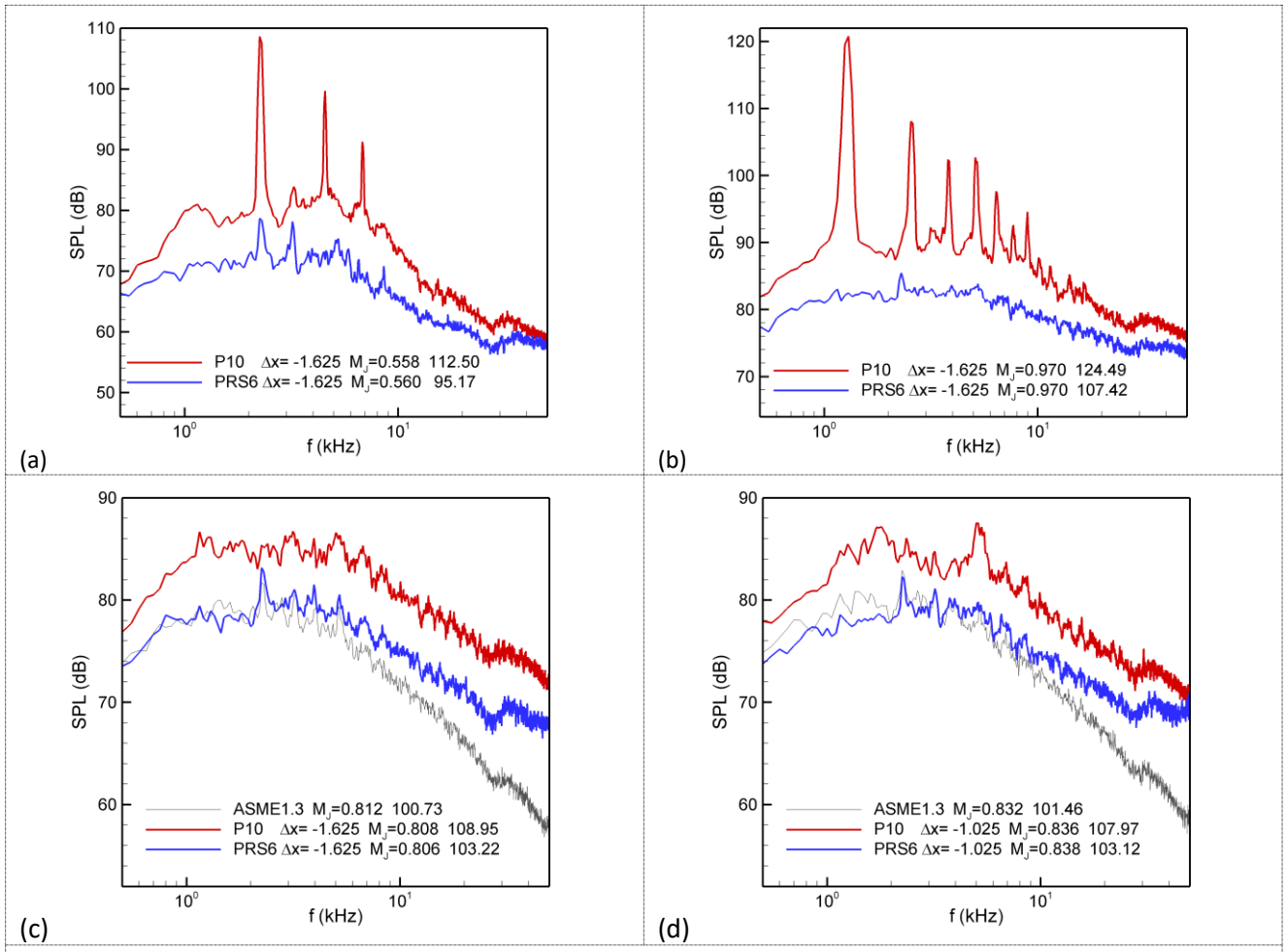

Fig. 16 SPL spectra at θ≈90° for the 10° conic plug demonstrating the effect of plug porosity on x-tone and EBBN; red lines: solid plug (P10), blue lines: porous plug (PRS6). Grey lines for data from ASME 1.3" nozzle. (a) M_J =0.59, △x=-1.625" (x-tone), (b) M_J =0.97, △x=-0.1.625" (x-tone), (c) M_J =0.81, △x=-1.625" (EBBN), (d) M_J =0.84, △x=-1.025" (EBBN).

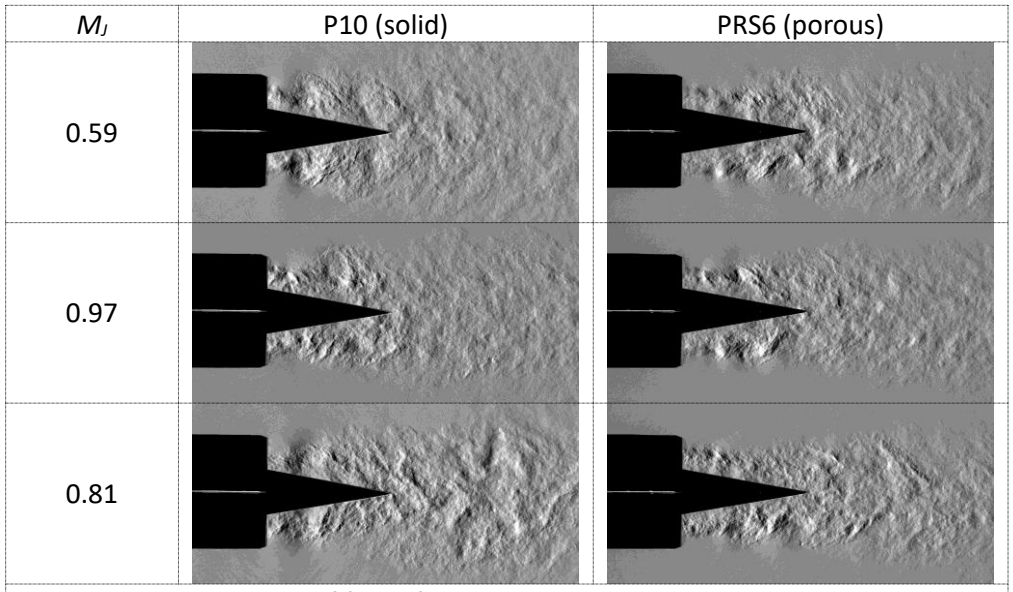

Fig. 17 Schlieren images of flows for the 10° conic plug corresponding to the noise data of Fig. 16 (a), (b) and (c); △x=-1.625”

.

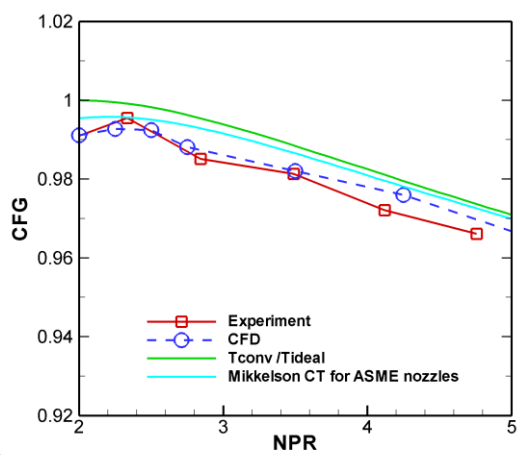

(a)

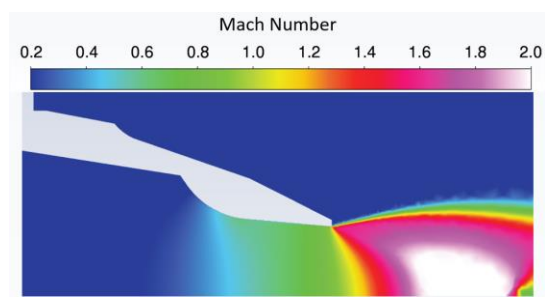

Mach number contours for NPR=4.25.

(b)

Fig. 18 Flow and thrust of D=1.3” ASME nozzle. (a) Thrust coefficient vs. NPR; red line: experimental data, blue dashed line: CFD prediction, green line: analytical prediction, light blue line: correlation for ASME nozzles from [11]. (b) An example of CFD results from which the *CFG* data are obtained, also showing the nozzle geometry.

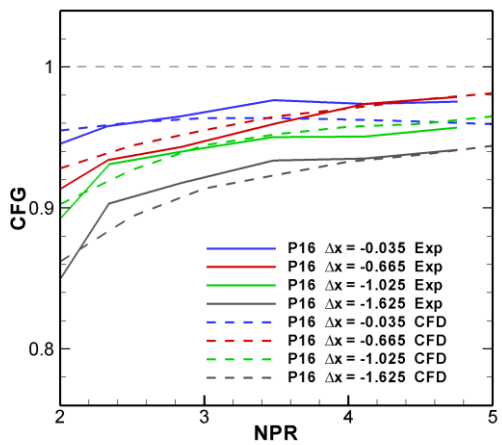

(a)

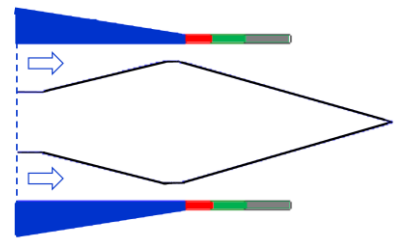

(b)

Fig. 19 Thrust coefficient of 16° conic plug for different lip extensions. (a) *CFG* vs. NPR; solid lines: experimental results, dashed lines: CFD results. (b) Schematic of the four lip extensions.

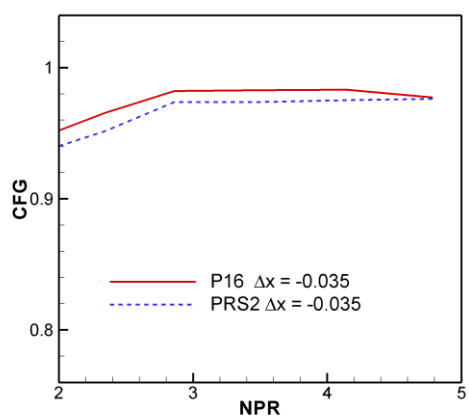

(a)

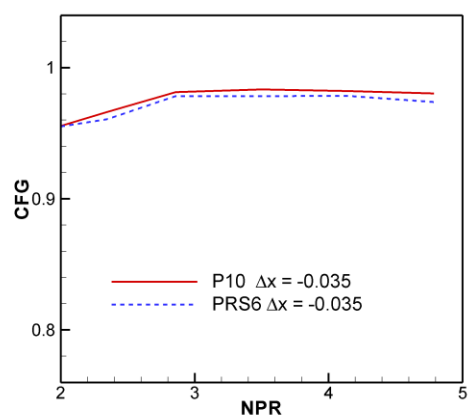

(b)

Fig. 20 Thrust coefficient vs. NPR showing plug porosity effect. Solid lines are for solid plugs while dashed lines are for corresponding porous plugs. (a) 16° conic case (P16 vs PRS2), (b) 10° conic case (P10 vs PRS6).